Full length article

Degradation of thermal transport properties in fine-grained isotropic graphite exposed to swift heavy ion beams

Alexey Prosvetov [a,b,*], Georges Hamaoui [c], Nicolas Horny [c], Mihai Chirtoc [c], Florent Yang [a], Christina Trautmann [a,b], Marilena Tomut [a,d,*]

[a] Materials Research Department, GSI Helmholtzzentrum, Planckstr. 1, 64291 Darmstadt, Germany
[b] Department of Materials and Earth Sciences, Technische Universität Darmstadt, Alarich-Weiss-Straße 2, 64287 Darmstadt, Germany
[c] Mechanical and Thermal Engineering Lab., ITheMM (EA 7548), Université de Reims Champagne Ardenne URCA, Moulin de la Housse BP 1039, 51687 Reims, France
[d] Institute of Materials Physics, WWU Münster, Wilhelm-Klemm-Straße 10, 48149 Münster, Germany

ARTICLE INFO

ABSTRACT

Isotropic polycrystalline graphite samples were irradiated with ~1 GeV ^{197}Au and ^{238}U ions of fluences up to 5×10^{13} ions/cm^2. Beam-induced changes of thermophysical properties were characterized using frequency domain photothermal radiometry (PTR) and the underlying structural transformations were monitored by Raman spectroscopy. The ion range (~60 μm) was less than the sample thickness, therefore thermal diffusivity contributions of the irradiated as well as non-irradiated layer were considered when analyzing the PTR data. At the highest applied fluences, the thermal effusivity of the damaged layer degrades down to 20% of the pristine value and the corresponding calculated values of thermal conductivity decrease from 95 Wm^{-1}K^{-1} for pristine material to 4 Wm^{-1}K^{-1}, a value characteristic for the glassy carbon allotrope. This technique provides quantitative data on thermal properties of ion-irradiated polycrystalline graphite and is very valuable for the prediction of lifetime expectancy in long-term applications in extreme radiation environments.

1. Introduction

The ongoing development of new generations of high-temperature nuclear reactors and high-power accelerators faces many technological challenges. One of the critical aspects is related to the extreme radiation and temperature operation conditions for engineering materials. In high-temperature gas cooled reactors (HTR), graphite acts both as moderator and as structural material, whereas in the field of high-power accelerators, it is the first choice material for collimators, beam dumps and production targets. For the latter application, one of the main limiting factors for higher luminosities is the degradation of the thermophysical properties of beam intercepting device materials exposed to high intensity beams. For high-dose applications, it is thus essential to understand how the thermophysical properties of different graphite grades evolve with accumulation of radiation damage.

Isotropic polycrystalline graphite (PG), a material that served traditionally for many decades in the nuclear field, is still one of the best candidates for applications in extreme radiation environments [1–3]. The low atomic number and density of graphite lead to reduced energy deposition by the ion beam in comparison with metals [4]. In addition, both the nuclear activation by interaction with high-energy primary ion beams and its decay time are low for pure carbon, qualifying graphite as most favorable in terms of radiation safety [1,5]. However, it was shown that heavy ion irradiations lead to beam-induced structural defects, phase transformations and degradation of the electrical and mechanical properties of graphite [6–10]. One has also to expect a severe influence of ion irradiation on the thermophysical properties of graphite, affecting both the thermal diffusivity (a) and conductivity (k) with a direct consequence on the efficiency of the system to diffuse the energy deposited by the ion beam. Under extreme conditions, reduced a and k may lead to performance degradation and ultimately to failure of the device.

This study concentrates on new fine-grained, high density, isotropic graphite grades with improved mechanical properties and stability at elevated temperatures that are under continuous

---

* Corresponding authors at: Materials Research Department, GSI Helmholtz Center of Heavy Ion Research, Planckstr. 1, 64291 Darmstadt, Germany.
E-mail addresses: a.prosvetov@gsi.de (A. Prosvetov), m.tomut@gsi.de (M. Tomut).

development. Structural and morphological irradiation-induced modifications are known to be determined by the pristine graphite structure. The evolution of thermophysical properties with accumulated radiation dose is dependent on the starting degree of graphitization. Most of the previous studies on polycrystalline graphite concentrated on neutron irradiation induced damage produced by collisional displacement cascades, relevant for nuclear reactor applications [11–17]. The defect creation mechanism via elastic atomic displacements, characteristic for neutron and keV-MeV ion irradiations, is quite different from ions of MeV-GeV energy [18,19]. When high-energy heavy ions pass through matter, the energy loss is dominated by ionization and electronic excitation processes of the target atoms (electronic stopping). Defect creation occurs via energy transfer from the excited electronic subsystem by electron-phonon coupling to the atomic system. After having slowed down to MeV-keV energies, approximatively within the last 10 μm of the ion path, nuclear energy loss becomes more and more dominant, and damage is created via atomic displacement cascades due to elastic collisions. In contrast to electronic stopping, this process is highly efficient because of the direct conversion of deposited energy into atomic motion. A specific property of swift heavy ions is the fact that above a critical electronic energy loss, each projectile can produce a cylindrical damaged region along its path, the so-called ion track [20]. Tracks form easily in insulators whereas many metals are insensitive. Track diameters are typically of the order of a few nanometers, the precise value depends on specific material properties and increases with the electronic energy loss of the projectile. The evolution of the damage with increasing ion fluence follows the direct impact model [21] which considers that the integral damage increases linearly in the initial irradiation stage but evolves towards saturation if more and more tracks overlap.

At present it is not clear to which degree nuclear and electronic stopping contribute to the overall damage and consequent degradation of thermophysical properties in graphite. Experimentally this phenomenon has not yet been investigated thoroughly, because data of thermal properties are scarce for neutron irradiated graphite [13,16,22,23] and non-existing for graphite irradiated with low and high energy ions. This lack of experimental data is probably linked to the fact that the penetration depth of ions is rather limited (tens of nanometers for keV ions and up to about 100 μm for GeV ions) and the analysis by classical methods typically applied for bulk samples, such as Laser Flash Analysis (LFA) [24] or scanning thermal microscopy (SThM) [25] is not straightforward.

In this work, the modification of thermophysical properties of fine-grained, isotropic graphite samples irradiated with GeV Au and U ions was investigated using the photothermal radiometry (PTR) technique [26–31]. This method was chosen based on its previous successful application for thermal characterization of modifications in plasma-exposed graphite [32,33] and proton irradiated ZrC [34]. The technique provides access to the thermal effusivity, e, allowing the measurement of the effusivity of graphite as a function of ion fluence and the determination of thermal conductivity, k. Raman spectroscopy was performed on fractured sample cross-sections for monitoring structural modifications along the full length of the ion trajectories.

The obtained results for ion-beam induced thermal conductivity degradation are also important for future model calculations, because they can be used as a benchmark for computer models such as finite element and molecular dynamics simulations [35–39].

2. Experimental

2.1. Material

The investigation concentrated on fine-grained polycrystalline graphite using the high density SIGRAFINE® R6650 grade produced by SGL Carbon SE. According to the data sheet provided by the manufacturer, this is an isotropic graphite grade produced by isostatic pressing. The average grain size is 7 μm and the density is 1.84 g/cm^3 [40]. The disk-shaped samples with diameter of 10 mm were cut from a larger bulk piece and lapped from one side to reduce the sample disks to a thickness of 0.5–0.9 mm.

As reference of disordered carbon material, we used commercial low temperature SIGRADUR® K and high temperature SIGRADUR® G grades of glassy carbon (HTW Hochtemperatur-Werkstoffe GmbH) and arc evaporated amorphous carbon foil (aC) (ACF-Metals). For thermal analysis a 2-mm thick, pristine, disk-shaped, polycrystalline graphite SIGRAFINE® R6650 sample served as reference. The densities as provided in Table 1 are taken from the manufacturer's datasheets [40,41], whereas thermal diffusivity and specific heat capacity values were determined from laser flash analysis and differential scanning calorimetry (DSC) measurements, respectively (see below).

2.2. Ion irradiation

The irradiations of polycrystalline graphite SIGRAFINE R6650 samples were performed at room temperature with ^{197}Au ions (4.8 and 5.9 MeV/u) and with ^{238}U ions (4.8 MeV/u) at the M3-beamline of the M-branch at the UNILAC accelerator of GSI Helmholtz Center (Darmstadt, Germany). The applied fluence varied between 1×10^{11} and maximum 5×10^{13} ions/cm^2. The ion flux was kept constant to about 2×10^9 ions/(s·cm^2). This beam energy was selected to minimize sample activation and on the other hand to provide sufficiently large ion ranges for analysis. The range of the Au and U ions in graphite, which corresponds to the thickness of the beam modified layer, is between 50 and 70 μm, one order of magnitude less than the sample thickness. For both ion species, the evolution of the energy loss, dE/dx, along the ion trajectory in graphite shows a rather homogeneous energy deposition over tens of μm (see Section 3.1.). The sample and irradiation parameters including the energy loss at the sample surface, the mean energy loss and the range of the ions according to calculations using the SRIM-2010 code [42] are summarized in Table 2.

2.3. Sample characterization

After the irradiation, some of the high-fluence samples were notched from the non-irradiated side and fractured. No pieces chipped off and the whole fresh cross-section of the sample was exposed for Raman spectroscopy damage analysis, using
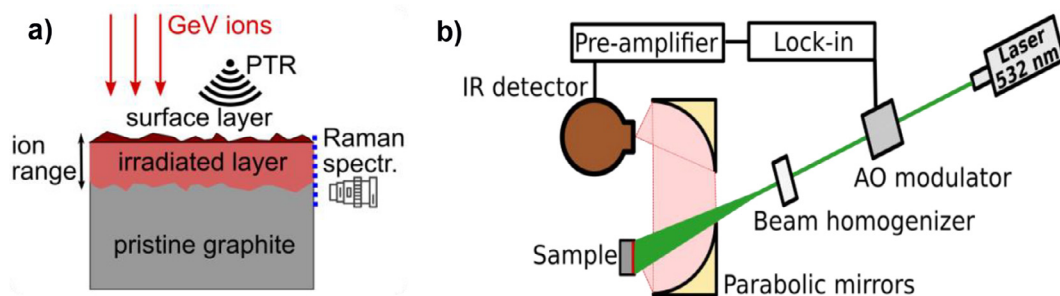
Table 1
Density of isotropic polycrystalline graphite and glassy carbon grades according to manufacturer's data sheets [40,41]; thermal diffusivity and specific heat capacity values were deduced from respective LFA and DSC measurements.

Material	Grade	Density (g/cm^3)	Thermal diffusivity (mm^2/s)	Heat capacity (Jg^{-1}K^{-1})
Polycrystalline graphite	SIGRAFINE R6650	1.84	80.8 ± 0.6	0.70
Glassy carbon	SIGRADUR K	1.54	1.3 ± 0.1	0.79
	SIGRADUR G	1.42	5.2 ± 0.1	0.81

Table 2

Sample thickness (L) and irradiation parameters including the specific ion energy (E_s) in units of MeV per nucleon (MeV/u), electronic energy loss at the sample surface $(dE/dx)_{surf}$, and mean energy loss $(dE/dx)_{mean}$ calculated by dividing the total kinetic energy by the ion range R (thickness of the irradiated layer) according to the SRIM-2010 code [42].

| Ion	E_s (MeV/u)	$(dE/dx)_{surf}$ (keV/nm)	$(dE/dx)_{mean}$ (keV/nm)	R (μm)	L (μm)	Fluence (ions/cm^2)
^{197}Au	4.8	20.3	16.6	57	486.0	1×10^{11}
					513.3	2×10^{11}
					513.0	5×10^{11}
					486.1	1×10^{12}
					511.4	1×10^{12}
					494.9	2×10^{12}
					496.2	1×10^{13}
					513.3	5×10^{13}
^{197}Au	5.9	19.9	17.1	68	506.8	1×10^{11}
					498.6	1×10^{12}
					507.8	1×10^{13}
					499.8	5×10^{13}
^{238}U	4.8	25.7	19.7	58	843.3	5×10^{11}
					871.5	1×10^{12}
					865.0	2×10^{12}
					907.4	5×10^{12}
					886.3	1×10^{13}
					930.2	5×10^{13}

Fig. 1. (a) Scheme of sample irradiation and analysis by means of photothermal radiometry (PTR) from top layer and by Raman spectroscopy from sample cross section; (b) Scheme of photothermal radiometry (PTR) setup.

line profiles along the whole ion range, including also a region of the non-irradiated substrate. The cross-section of the irradiated layer was additionally inspected using Schottky field emission scanning electron microscopes (Philips XL30 FEG for low magnification and JEOL JSM-7600F for high magnification). Ion beam-induced structural changes were analyzed by confocal Raman spectroscopy (HR800 system, Horiba Jobin Yvon) with a 20 mW laser of 473 nm excitation wavelength. The calibration of the spectrometer was done using a Si sample. The Raman spectra were recorded along five profiles on the sample cross-section, each with a length of 100 μm, normal to the irradiated surface and along the incoming ion direction, with a step of 2 μm, using spectral autofocus. The scheme of an irradiated sample and the orientation of the different measurement techniques are shown in Fig. 1a.

To analyze the thermophysical properties of the irradiated layers, all samples were measured using a frequency domain photothermal radiometry (PTR) setup. The sample surface is heated with a continuous laser (DPSS, Dream Lasers Technol. Co., model SDL with a wavelength of 532 nm) modulated in the frequency domain via an acousto-optic modulator (AOM model AA.MTT.AR 05) in the frequency range of 1 to 100 kHz. At these frequencies, the measurements are subject to 3D effects which necessitate a change of the laser beam shape. At low frequencies a flat top (FT) optics, consisting of a beam shaper/diffuser (ED1-C20, Ø1″ 20° Circle Pattern Diffuser, Thorlabs) and two lenses, is used. One lens collects the large scattered beam and the other focuses it on the

sample. With this configuration, the laser spot size is larger than the sample which imposes a 1D heat transfer throughout the material as explained in numerous earlier studies [28,34,43,44]. The infrared radiation emitted from the sample surface is transferred by two off-axis parabolic gold-coated mirrors to a liquid-nitrogen cooled HgCdTe photoconductive detector sensitive for IR radiation wavelength between 5 and 12 μm. The detector output signal is analyzed by a lock-in amplifier Stanford Research Systems SR865. The signal is proportional to the variation of the temperature of the sample surface and is linked to the thermophysical properties of the investigated material layers. The experimental setup is sketched in Fig. 1b, and more technical details are given elsewhere [28].

To provide input data for the PTR analysis, the thermal diffusivity and heat capacity of a 2-mm thick pristine graphite sample (see Table 1) were determined by means of laser flash analysis (LFA) on a NETZSCH LFA427 device [45,46]. The surface roughness of this sample was measured using a Dektak profilometer from Veeco with a tip radius of 12 μm. In the LFA set-up the rear face of a given sample was illuminated with a 0.3 ms laser pulse (laser wavelength $\lambda = 1064$ nm) and the relative temperature evolution on the sample front face was recorded with a cooled IR detector. Thermal diffusivity values were deduced based on the half-time, a characteristic time at which the temperature at the sample front face reaches half of the maximum rise, taking into account the finite pulse length and heat losses of the sample [47,48].
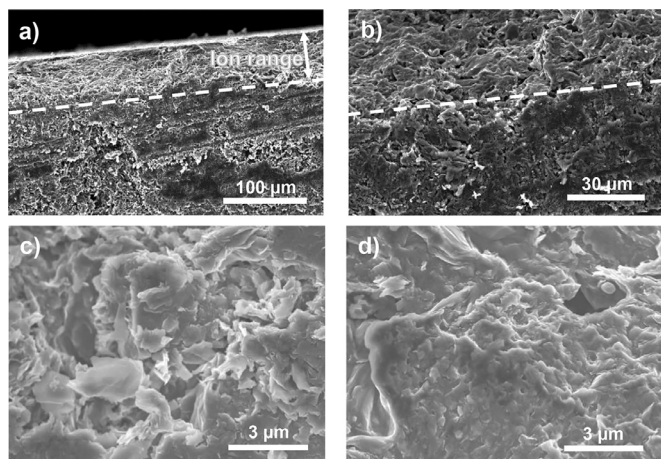
Fig. 2. SEM images of graphite sample irradiated with 4.8 MeV/u U ions at a fluence 5 × 10¹³ ions/cm². (a) and (b) are low magnification images of sample cross-sections, the dashed line marks the SRIM calculated ion range (upper area: irradiated and lower area: pristine); (c) high magnification image of non-irradiated section (beyond ion range); (d) irradiated area of graphite sample within ion range.

3. Results and discussion

### 3.1. Morphological and structural changes

For all studied samples, scanning electron microscopy (SEM) images show distinctive contrast features in the cross-section of the irradiated layer. Examples of low and high magnification SEM images of a sample irradiated with 5 × 10¹³ U ions/cm² are presented in Fig. 2. On the low magnification image in Fig. 2a and 2b the irradiated layer features brighter structures. The thickness of this modified layer is in good agreement with the ion range as calculated by the SRIM-2010 code (dashed line). Compared to the non-irradiated substrate (below dashed line), the material of the ion-modified layer (above dashed line) seems to have a more homogeneous structure, showing some signs of brittle fracture. The brighter features observed in this layer correspond to the complex topography of the fractured surface producing more

secondary electrons in the SEM detector. In the high-magnification SEM images (Fig. 2c and d), the pristine graphite displays a polycrystalline structure with sharp edges of individual graphite flakes whereas the irradiated graphite shows smoothed conglomerates of grains with no defined edges. This indicates possible bending and cross-linking of basal planes in the irradiated layer leading to a particular interconnected carbon structure.

Raman spectroscopy analysis allowed us to distinguish between the structure of the irradiated layer and the pristine substrate and to check if the graphite exposed to swift heavy ions still preserves the sp^2 bonding. The measurements were performed on the cross section of fractured samples by stepwise recording spectra from the sample surface, across the irradiated region until deep into the non-irradiated substrate with a step width of 2 μm. An example of a Raman spectroscopy depth profile for a sample irradiated with 4.8 MeV/u U ions at a fluence 5 × 10¹³ ions/cm² is shown in Fig. 3. The spectra are background corrected and normalized to the intensity of the G-band (Raman shift 1582 cm⁻¹). The position of the sample surface was identified based on the appearance of the G-band in the spectrum. The corresponding point was set as 0 depth for each line in the depth profile. Because of the finite laser beam spot size (~4 μm) and the surface roughness of the fractured sample, the real sample edge is defined within an uncertainty of several μm. To analyze the spectra along the full scan length, the ratio of D- and G-band intensities I(D)/I(G), the full width at half maximum of the G-band FWHM(G) and the intensity ratio of the so called D3-band (around 1500 cm⁻¹) to the G-band I(D3)/I(G) were taken into account. Details of the Raman spectra fitting and more examples of spectra measured on the polycrystalline graphite irradiated with 4.8 MeV/u Au and U ions at a fluence of 1 × 10¹², 1 × 10¹³ and 5 × 10¹³ ions/cm² can be found in Section 1 of the Supplemental Material. The parameter I(D)/I(G) is connected to the in-plane crystallite size and to the defect density in basal planes, whereas FWHM(G) describes the degree of crystalline order of the investigated carbon material [49–51]. The D3-band is usually assigned to the presence of amorphous carbon [52,53]. A small shift of the G-peak position at the end of the ion range is ascribed to beam-induced stresses at the interface between the pristine and the irradiated part (see Fig. 3b)
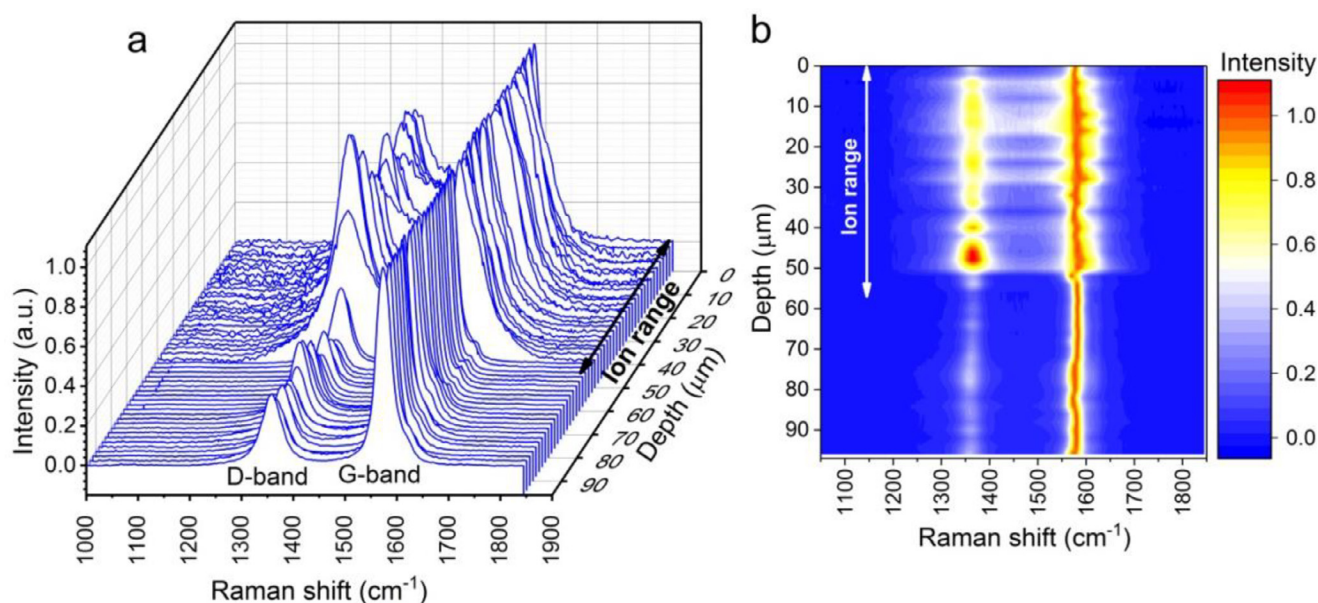
Fig. 3. Raman spectra of isotropic graphite sample irradiated with 4.8 MeV/u U ions at a fluence of 5 × 10¹³ ions/cm². The spectra are normalized to the intensity of the G-band. (a) Depth evolution of spectra as 3D plot; (b) corresponding 2D intensity map with intensity as color code.
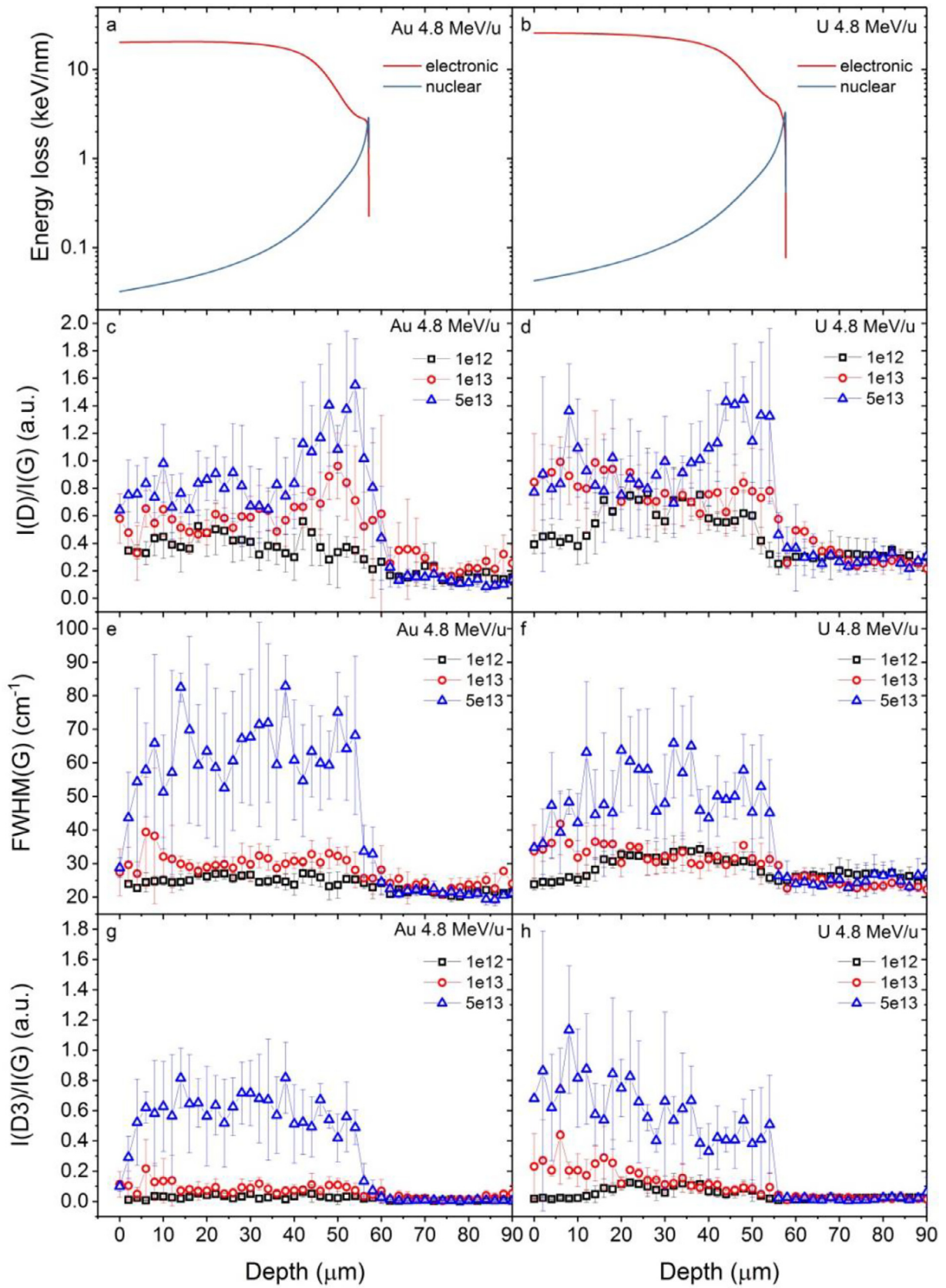
Fig. 4. Electronic and nuclear energy loss of 4.8 MeV/u Au ions (a) and U ions (b) in polycrystalline graphite and the respective I(D)/I(G) ratio (c, d), FWHM(G) (e, f) and I(D3)/I(G) ratio (g, h) averaged over five line profiles measured on fractured cross-section of samples exposed to fluences of 1×10^{12}, 1×10^{13} and 5×10^{13} ions/cm^2.
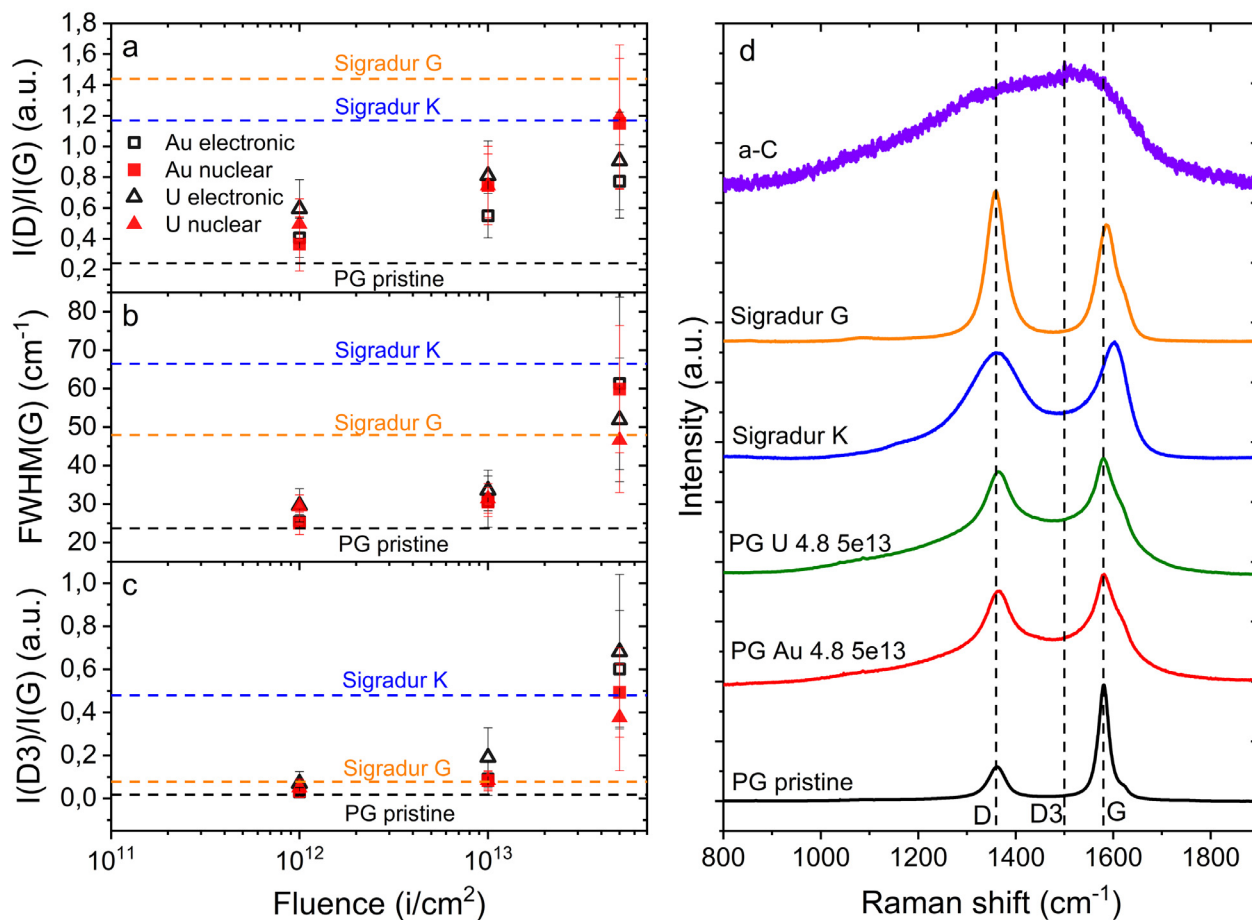
Fig. 5. Evolution of Raman parameters (a) I(D)/I(G), (b) FWHM(G) and (c) I(D3)/I(G) with increasing fluence of Au and U ion irradiated polycrystalline graphite. Open symbols are averaged values from 0 - 40 μm sample depth dominated by electronic stopping and full symbols are averaged values from 40 - 56 μm sample depth dominated by nuclear stopping. The average values of pristine polycrystalline graphite and two kinds of glassy carbon are marked by dashed lines. (d) The average Raman spectra of pristine polycrystalline graphite (PG pristine), PG irradiated with 5×10^{13} ions/cm^{-2} Au and U ions, two grades of glassy carbon (Sigradur K and Sigradur G) and amorphous carbon (a-C).

For fluences of 1×10^{12}, 1×10^{13} and 5×10^{13} ions/cm^2, the depth profiles of these parameters along with the calculated energy loss of 4.8 MeV/u Au and U ions are presented in Fig. 4. For all measured samples, the profiles of the three studied Raman parameters follow a similar scheme. The fluctuations along the profile are ascribed to the rather large grain size (~7 μm) of the sample being larger than the size of the laser spot (~4 μm) of the Raman spectrometer. Within the first ~55 μm from the irradiated surface, the I(D)/I(G), FWHM(G) and I(D3)/I(G) values are larger than those for pristine graphite. Towards the end of the ion range, both values steeply drop to the average values of pristine polycrystalline graphite within less than 10 μm. The high I(D)/I(G), FWHM(G) and I(D3)/I(G) values in the irradiated layer are a clear evidence for structural changes and disordering of the carbon lattice. The thickness of this beam-modified layer is in good agreement with the range of the ions as calculated by the SRIM-2010 code. For both irradiations (Au and U ions), the values of the I(D)/I(G) ratio increase at a sample depth of approximately 50 μm (Fig. 4c and d) following the trend of nuclear stopping. This correlation indicates a dominant contribution of point defects due to the nuclear energy loss at the end of the ion range. In contrast, the values of FWHM(G) and I(D3)/I(G) are almost constant within the whole ion range, steeply decreasing close to the depth where the ions stop, suggesting a correlation to the electronic energy loss without excluding some contribution by the nuclear energy loss. The loss of crystalline order, indicated by larger values of

FWHM(G) and the formation of amorphous carbon (I(D3)/I(G)) is significantly more pronounced at the highest fluence (5×10^{13} ions/cm^2). In spite of high defect density and disordering, the corresponding Raman spectra still show the predominance of sp^2 bonds, characteristic to graphite basal planes. In order to better distinguish the specific contributions of the electronic and nuclear energy loss, the studied Raman parameters were averaged along the first 40 μm from the surface (electronic dE/dx) and for the depth range from 40 to 56 μm (nuclear dE/dx). The mean values for the various fluences are presented in Fig. 5.

The analysis of the Raman spectra of the graphite samples irradiated at the highest fluence of 5×10^{13} ions/cm^2 with Au and U ions indicate a beam-induced transition from fine grained polycrystalline graphite to a damaged structure similar to glassy carbon (Fig. 5). Glassy carbon is a fullerene-related structure of randomly interconnected tortuous graphitic lamellae of sp^2 bonded carbon [54–57]. In general the structure of glassy carbon strongly depends on the process temperature during pyrolysis, which can extend from 600 °C to 2500 °C. Low temperature grades of glassy carbon are characterized by small size, disordered sp^2 bonded carbon domains, which tend to rearrange and form larger and less-disordered curved flakes in a high temperature pyrolysis process. The production process temperature of the Sigradur K and Sigradur G samples used in this work is unknown, but one can compare the Raman spectra of these samples with those from a previous study [56] and qualitatively define them as low and high

temperature grades respectively. According to the data sheet of the manufacturer [41], the two grades differ also in maximum service temperature of 1000 °C for Sigradur K and of 3000 °C for Sigradur G. We consider these two grades as examples of two extreme cases but are aware that depending on the synthesis conditions other intermediate grades exist. The values of I(D)/I(G), FWHM(G), I(D3)/I(G) (Fig. 5. (a), (b) and (c) respectively) and the shape of the Raman spectra (Fig. 5. d) of our high fluence irradiated graphite become rather close to the typical low-temperature glassy carbon characterized by smaller, disordered sp^2 building blocks.

The observed structural changes of swift heavy ion irradiated polycrystalline graphite show a similar trend to the previously studied evolution of highly oriented pyrolytic graphite (HOPG) exposed to low [51,58] and high [59,60] energy ions, as well as to low energy ion irradiated polycrystalline graphite [15] and glassy carbon [61]. All this data indicates a high sensitivity of sp^2 based carbon structure to the radiation damage dominated by nuclear energy loss. The elastic collisions and the resulting damage cascades lead to the development of dislocations, milling and misorientation of carbon crystallites, reaching finally a highly disordered turbostratic structure and complete amorphisation at a very high fluence (~1 × 10^{16} ions/cm^2) as supported by HRTEM analysis [15].

The effect of electronic energy loss on the damage creation in graphite has not yet been studied sufficiently. The direct comparison of our results with data of Ref. [59,60] is complicated because of different experimental conditions. By comparing of I(D)/I(G) values the dependence of the Raman D-band intensity on the energy of an excitation laser E_L should be considered by using a scaling factor of E_L^4 [50]. The Raman spectra of polycrystalline graphite at a fluence of 5 × 10^{13} ions/cm^2 show more significant structural disorder and a higher fraction of amorphous carbon in comparison with ion irradiated HOPG. This can be connected to the initial structural difference between polycrystalline graphite and HOPG. Polycrystalline graphite is formed of randomly oriented small grains, consisting of multiple crystallites of well-structured graphite. Although on the scale of single crystallites this material has the structure of ideal HOPG, the initial defected structure, microscopic crystallite and grain sizes, as well as quasi-isotropic properties due to random orientation of anisotropic grains may cause a different response of PG and HOPG to swift heavy ion irradiation.

The present Raman analysis allows us to conclude that polycrystalline graphite shows pronounced defect formation towards the end of the ion range ascribed to nuclear energy loss. In the entire electronic energy loss regime, strong effects on the structural changes were observed, but the data do not provide evidence if and to which extend this is a result of a combined contribution of nuclear and electronic energy loss. The data are also not conclusive enough to discuss synergistic effects between the electronic and nuclear energy loss as previously reported for oxides [62–66].

3.2. Thermophysical properties

Modulated heating of a material leads to the generation and propagation of so-called thermal waves [26]. The penetration depth of the thermal waves defines the probing thickness at a given frequency and is known as the thermal diffusion length $\mu = \sqrt{a/\pi f}$, where a is the thermal diffusivity of the studied material and f the laser excitation frequency modulation. With a PTR setup configuration combined with a beam diffuser as described above, heating is considered to be one-dimensional (1D). A detailed theoretical descriptions of the method and its limitations can be found in Refs. [28,34,43,67].

Table 3
Thermal effusivity e of pristine graphite (SIGRAFINE R6650) from laser flash analysis and PTR results for e and $L \cdot a^{-1/2}$ of cut and lapped surface layers.

| Pristine graphite	Method	e (Ws$^{1/2}$m^{-2}K^{-1}, × 10^3)	$L \cdot a^{-1/2}$ (s$^{-1/2}$, × 10^{-3})
Bulk	LFA	11.6 ± 1.2	–
Cut surface	PTR	2.9 ± 0.6	3.0 ± 0.1
Lapped surface	PTR	4.2 ± 0.9	1.3 ± 0.1

The modulated heat transfer through our multi-layered system was simulated using a 1D thermal quadrupoles method [68] and the experimental PTR data (normalized amplitude and phase simultaneously) were fit by means of a Gauss-Newton algorithm. For more details on selecting a multi-layer system for describing the irradiated samples see Section 2a of the Supplemental Material. Based on the theoretical approaches presented in previous works [34,44], the following independent parameters are considered: (1) the ratio of thermal effusivities e_i/e_{i+1} and (2) the product $L_i a_i^{-1/2}$, where the subscript i stands for the layer number i and L_i and a_i denote the layer thickness and its thermal diffusivity, respectively. Knowing that e is a function of the thermal conductivity k_i, density ρ_i, and specific heat capacity C_{Pi} of each layer, the effusivity is $e_i = \sqrt{k_i \rho_i c_{pi}}$.

Additionally, the estimated sensitivity of the amplitude and phase to all independent parameters of the theoretical model were calculated and presented in the Supplemental Material Section 2b (Figs. S4 and S5). The sensitivity analysis for the non-irradiated samples (Fig. S4) shows a perfect correlation between e of the surface and substrate layer, with the consequence that just the ratio of e could be obtained and that it is impossible to extract them simultaneously as fitting values. Thus, the value of e of bulk graphite SIGRAFINE R6650 was determined in an independent experiment by means of LFA, yielding $a = 8.1 \times 10^{-5}$ m^2/s and $C_p = 704$ Jkg^{-1}K^{-1}. Inserting $\rho = 1.84$ g/cm^3 for the bulk density of pristine graphite from the material datasheet [40], a value of $e = 11.6 \times 10^3$ Ws$^{1/2}$m^{-2}K^{-1} is obtained. In order to calculate e of the non-irradiated graphite substrate, the LFA results were used as input parameters in the 1D PTR heat transport model. The obtained parameters are summarized in Table 3 considering that the uncertainties of the PTR fitting are calculated according to the procedure described in [69] and detailed in the Supplemental Material Section 2c using 10% uncertainty on the input parameters of the model.

The specific nature of the surface layer is not the main object of this study, however the effect of graphite grain size is presented in the Supplemental Material Section 3. It should be mentioned that near-surface structural effects, like crystallite refinement and residual stress [70], as well as increased hardness [71] were reported earlier for machined synthetic graphite.

Selected PTR data of fluence series of graphite samples irradiated with Au and U ions are presented in Fig. 6 showing the normalized amplitude and phase of the PTR signal as a function of frequency. The evolution of the amplitude and phase in the scanned frequency range changes with accumulated ion fluence, indicating irradiation-induced modifications of the thermophysical properties. Since the change of emissivity with fluence is negligible, the change of amplitude is directly related to the modified thermal properties of the samples. Overlapping of the curves, observed at low ion fluences, indicates a similar thermal response from different samples and a small beam effect on thermophysical properties. At the highest fluence, the evolution of the amplitude and phase curves in the mid and high frequency regime indicates homogenization of the irradiated layers.

From the data shown in Fig. 6 in combination with the theoretical model, the fitting parameters e_{surf},
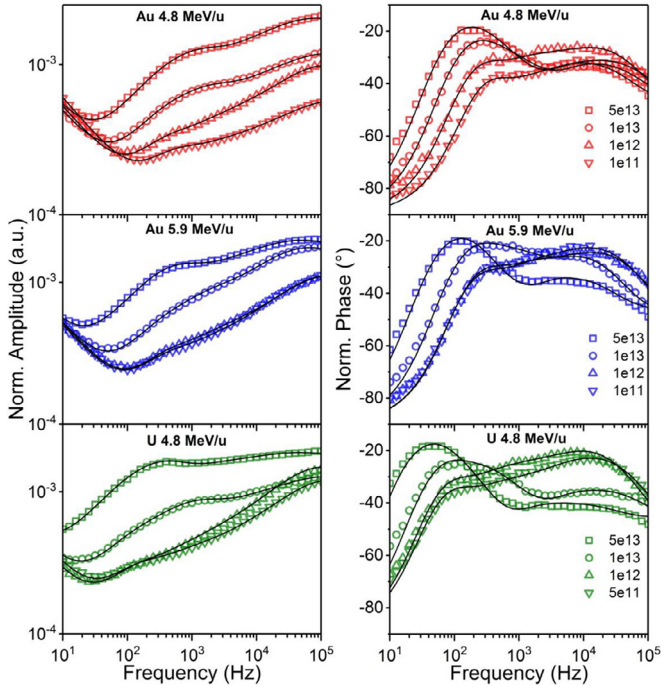
Fig. 6. Series of PTR data for isotropic polycrystalline graphite samples irradiated with Au ions (4.8 and 5.9 MeV/u) and with U ions (4.8 MeV/u) of various fluences: normalized amplitude and phase of the thermal signal as a function of frequency. Solid lines are model fits considering a 3-layer system.

Fig. 7. Thermal effusivity (top) and $La^{-1/2}$ (bottom) values versus fluence as deduced from fits to experimental PTR data: surface layer (open symbols) and irradiated layer (full symbols) for polycrystalline graphite samples exposed to different Au and U ion beams.

e_{irr}, $(La^{-1/2})_{surf}$, and $(La^{-1/2})_{irr}$ were extracted. The evaluation considers the sensitivity analysis of Fig. S5 using as input parameters the properties of the substrates (taken from LFA Table 3 results) and the thickness of the layers (see Table 2). The SRIM ranges were used as thicknesses of the irradiated layers with the assumption that the ion range does not change with fluence and that the radiation damage of the irradiated layer along the ion range in first approximation is quasi homogeneous, supported by the Raman investigation presented above. The results of these thermophysical properties are presented in Fig. 7.

From Fig. 7 it is clearly seen that the accumulation of ion fluence leads to degradation of e and to an increase of $La^{-1/2}$ for both layers (exhibiting a similar trend). Therefore, the overall increase in amplitude with increasing fluence (Fig. 6) is ascribed to an overall higher surface temperature due to a decrease in thermal effusivity and thus thermal conductivity. The decrease of e and increase of $La^{-1/2}$ with ion fluence for the surface and for the irradiated layer is probably mainly caused by the degradation of the thermal diffusivity a and thus of the thermal conductivity k of the layer. At the highest fluence of 5×10^{13} ions/cm^2, e_{irr} tends towards the typical value for glassy carbon (~1500–2600 Ws$^{1/2}$m^{-2}K^{-1}) calculated based on the data for SIGRADUR K and SIGRADUR G taken from Table 1. The unknown structure of the surface layer makes further deconvolution of each term of the parameter $La^{-1/2}$ difficult because this layer was hardly distinguished by means of Raman spectroscopy, optical microscopy and SEM. Nevertheless, it is reasonable to assume that the thickness of the surface layer is of the order of the surface peak-to-valley roughness and at least an order of magnitude less than the ion range. Since the thermal diffusivity a derived from $La^{-1/2}$ depends on the thickness at a power of 2, large thickness uncertainties cause large errors. Nonetheless, previous studies have shown that beam-induced swelling in a porous material such as graphite is only of the order of 1%. Swelling of individual crystallites may be more pronounced but is assumed to be readily accommodated
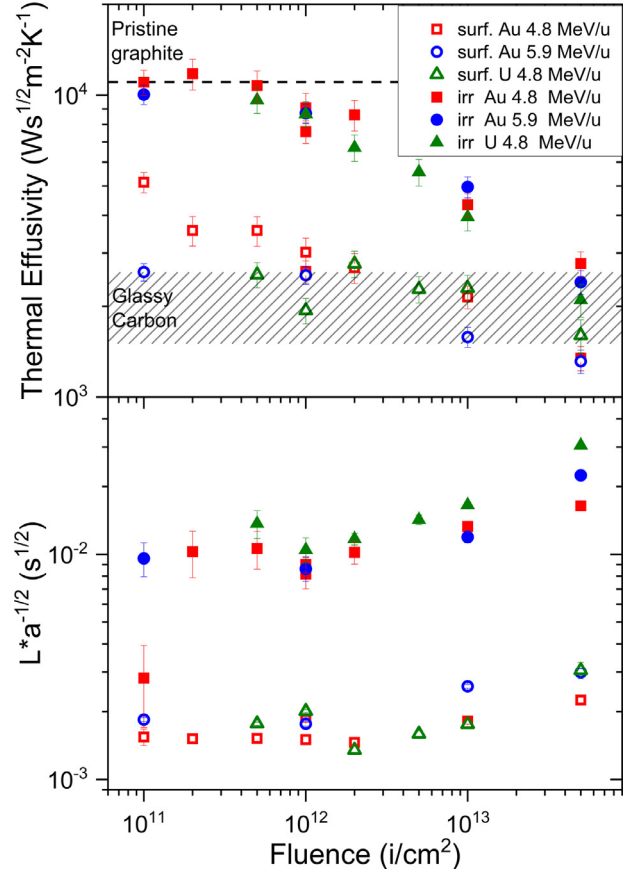
by the existing porosity [72]. This indicates that a thickness variation of the irradiated layer can be neglected throughout our calculations. Subsequently, the product $La^{-1/2}$ describes mostly qualitatively the degradation of a. A quantitative analysis should rely on the fitted values of thermal effusivity instead.

The observed changes of the thermophysical properties of our irradiated polycrystalline graphite samples are ascribed to beam-induced structural changes, as deduced from Raman spectroscopy. It is assumed that in the electronic energy loss regime, each projectile creates a nanometric track. This direct impact process means that at low fluences the structural changes increase linearly with fluence until individual tracks start to overlap with neighboring tracks. Finally, at high fluences, when the whole sample is completely covered by tracks, the material modification reaches a saturation limit. This direct impact phenomenon is typically described by the following exponential function [21]:

$$Y = 1 - A\left(1 - e^{-\sigma\Phi}\right) \tag{1}$$

where Y denotes the material modification, A is the amplitude of the degradation in the saturation regime at high-fluence, σ is the damage cross-section of a single ion, and Φ is the ion fluence. If the damage along the ion path is continuous, one can deduce the corresponding track radius R from the damage cross-section $\sigma = \pi R^2$. To estimate the size of the tracks created by Au and U ions used in this experiment, Eq. (1) was applied to fit the thermal effusivity data of the irradiated layer shown in Fig. 7. The relative e degradation ($e_{irr}/e_{pristine}$) as a function of fluence and the corresponding fit values are presented in Fig. 8a and in Table 4,
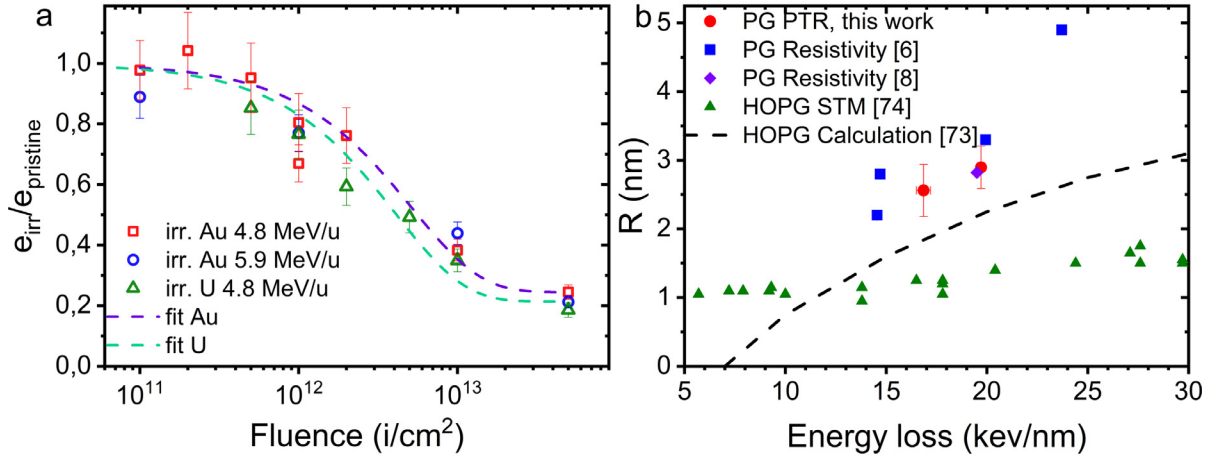
Fig. 8. (a) Ratio of thermal effusivity of irradiated to pristine layer as a function of fluence. Symbols represent experimental data, dashed lines are exponential fits of the data series corresponding to samples irradiated with Au (violet) and U (green) ions; (b) Track radii as a function of the average total energy loss, comparing present results with previous experimental and theoretical data for polycrystalline graphite and for highly oriented pyrolytic graphite (HOPG). The dashed line corresponds to thermal spike calculations [73].

Table 4
Track parameters deduced from exponential fits to beam-induced thermal effusivity data as a function of fluence according to Eq. (1). The data for 4.8 and 5.9 MeV/u Au ion are fitted together.

Ion	Amplitude A	Cross section σ (nm²)	Track radius R (nm)
^{197}Au	0.76 ± 0.04	20.6 ± 6.1	2.6 ± 0.4
^{238}U	0.79 ± 0.04	26.4 ± 5.6	2.9 ± 0.3

respectively (the data for 4.8 and 5.9 MeV/u Au ions are shown combined because of their similar energy loss (see Table 2)).

The deduced damage cross-section and the respective track radius of U ions are slightly larger than the values for Au ions (Table 4), which is in agreement with the fact that the energy loss of U ions is higher. The damage cross sections obtained in this work are comparable with values deduced from on-line electrical resistivity measurements of irradiated polycrystalline graphite [6,8] (Fig. 8b). This agrees well with the assumption, that both the electrical and thermal conductivities have a similar sensitivity to ion beam induced defects. The track radii for the irradiated polycrystalline graphite are systematically higher in comparison with reported values for highly oriented pyrolytic graphite (HOPG) obtained by thermal spike model calculations [73] and from investigations by scanning tunneling microscopy (STM) [74]. The higher damage cross-sections of fine grained graphite compared to the thermal spike model calculations for HOPG are probably due to the structural difference, as discussed in Section 3.1. This leads to an opposite effect to the generally accepted positive impact of grain boundaries in annihilation of mobile defects in collision radiation damage studies. When comparing the experimental track radii, it has to be considered that STM measurements record the convoluted information from beam-induced topography and local density of electronic surface states, probing thus a different volume than tracks in bulk graphite. The data deduced from our PTR analysis provide supportive evidence for the conclusion that track radius in polycrystalline graphite corresponding to a modified thermophysical property seems to be homogeneous along the whole ion range. We conclude this from the PTR measurements where by frequency scanning, different depths of the irradiated sample are probed showing that the applied 3 layer model containing a single irradiated layer with homogeneous properties for both electronic and nuclear energy loss dominated sections can very well fit the experimental data.
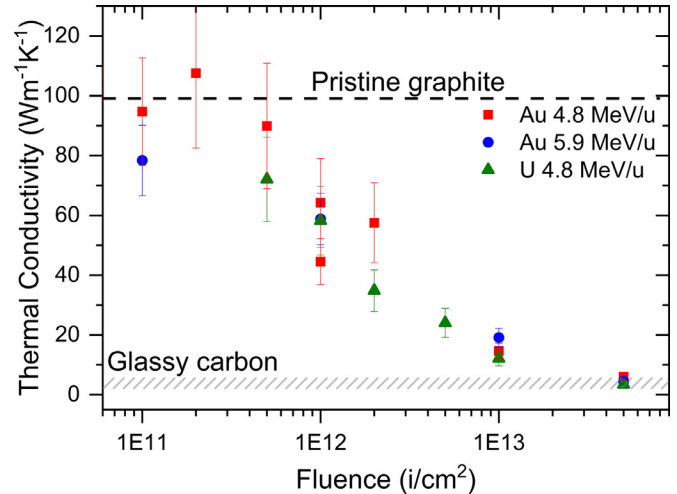
Fig. 9. Degradation of thermal conductivity of graphite as a function of fluence. The data were deduced from thermal effusivity measurements assuming that the pristine value of the volumetric heat capacity does not change significantly.

As the thermal effusivity is a function of the thermal conductivity and volumetric heat capacity of a given material, the contribution of these parameters in the observed beam-induced decrease of e can be estimated. The change of the density of such material is omitted because swelling can be neglected as mentioned above. Based on results from neutron irradiation [75], it is also possible to assume that beam-induced changes of the heat capacity can be neglected. It means that the main contribution of the thermal effusivity degradation is due to the decrease of the thermal conductivity.

For technical/practical applications it is more common to consider the thermal conductivity rather than the thermal effusivity. As discussed above, the determination of k from $La^{-1/2}$ is affected by large errors on the thickness. Therefore in order to quantitatively estimate this parameter, it was calculated from the measured e value using $e_i = \sqrt{k_i \rho_i c_{pi}}$. Inserting the volumetric heat capacity of pristine graphite and a constant density, k evolves as a function of fluence as shown in Fig. 9. For the Au as well as the U beams, k drops from ~100 Wm^{-1}K^{-1} originally, down to 3–5 Wm^{-1}K^{-1} for the highest fluence of 5 × 10^{13} ions/cm². Additionally, it should be noted that the density difference between

polycrystalline graphite and glassy carbon is about 20%. Thus, even if complete transformation at the highest fluence is assumed and the lower density of glassy carbon is taken into account, the final k will increase just by a few $Wm^{-1}K^{-1}$ being an order of magnitude less than the value of pristine polycrystalline graphite.

As for the case of effusivity, the strong degradation of the thermal conductivity with increasing fluence is in good agreement with structural transformations in irradiated graphite observed by Raman spectroscopy. The large number of defects produced along the entire length of the projectile path has a strong influence on the properties of graphite. Previous molecular dynamics simulations showed that carbon materials have the tendency to recrystallize into faulty sp^2 structures with non-6-membered carbon rings during the ultrafast cooling of the lattice in the ion tracks [38]. Such defects induce fragmentation, bending, and interconnections of basal planes, but the predominant sp^2 structure is retained.Taking into account that the main heat carriers in graphite are phonons [76–80], the degradation of k is ascribed to a decrease of the phonon mean free path due to enhanced phonon scattering at defects and newly formed grain boundaries. This is supported by the finding of Fugallo et al. [76] who demonstrated a pronounced decrease of the lattice thermal conductivity of graphene and graphite when the crystallite size becomes smaller than 10 μm. Irradiation-induced point defects have also an important contributions to the degradation of thermal conductivity in graphene and graphite, as shown by means of molecular dynamics simulation [36,81].

A comparison of the degradation of k induced by neutron irradiation was done based on the dpa calculation of collisional-cascade induced displacements along the ion trajectory. For the highest fluences of 5×10^{13} ions/cm², the dpa values calculated using SRIM-2008 Kinchin-Pease Quick [82] with an displacement energy of 25 eV [39,83] are of the order of 10^{-3} for the first 80% of the irradiated layer thickness, increasing gradually to a value of 5×10^{-2} for the last 20% of this layer. The relative change of the thermal conductivity of our graphite samples induced by swift heavy ions is larger than the one caused by room temperature neutron irradiations at the same dpa value [13,22]. This indicates that elastic collisions are not the only responsible mechanism for the degradation of the thermal conductivity of swift heavy ions irradiated graphite, where the damage creation by the indirect mechanism of ionization/excitation and coupling to the crystalline lattice play also an important role.

4. Conclusions

The irradiation of polycrystalline isotropic graphite with swift heavy ions (4.8 and 5.9 MeV/u Au and 4.8 MeV/u U) in the electronic energy-loss regime leads to significant structural damage and modifications of thermophysical properties. Analysis of the irradiated sample cross-sections by Raman spectroscopy and SEM provide clear evidence of defect production and at high fluences of a transition towards a glassy carbon-like material. To quantify the radiation-induced effects on thermal effusivity and thermal conductivity, the technique of frequency domain photothermal radiometry in combination with a three-layer model was successfully applied. The analysis of the relative effusivity degradation shows a single ion impact mechanism of the accumulated radiation damage with a track diameter of 5–6 nm. For future application of graphite in high-dose environments, it is important to emphasize that, at high ion fluences corresponding to complete track overlap (5×10^{13} ions/cm²), the thermal effusivity of the irradiated material drops down to approx. 20% of the pristine value. The corresponding values of thermal conductivity, obtained from the latter parameter assuming no beam-induced changes in volumetric heat capacity, decrease from 95 to approximately

$4 \ Wm^{-1}K^{-1}$, which is in close agreement with glassy carbon k values. Such a tremendous degradation can lead to inefficient heat dissipation and finally to thermomechanical failure of graphite beam dumps and production targets in ion accelerators. The risk due to largely reduced thermal conductivity values in high-dose environments have to be considered when designing and estimating the long-term operation conditions of beam-intercepting devices for the new generations of high power accelerators such as the Facility for Antiproton and Ion Research (FAIR) in Darmstadt, the High Luminosity Large Hadron Collider (HL–LHC) and the Future Circular Collider (FCC), both at CERN in Geneva.

Declaration of Competing Interest

The authors declare that they have no known competing financial interests or personal relationships that could have appeared to influence the work reported in this paper.

Acknowledgements

Supplementary materials

Supplementary material associated with this article can be found, in the online version, at doi:10.1016/j.actamat.2019.11.037.

References

[1] H. Geissel, M. Winkler, H. Weick, K. Behr, G. Münzenberg, H. Simon, K. Sümmerer, B. Achenbach, D. Acker, D. Ackermann, T. Aumann, J. Äystö, R. Baer, M. Berz, D. Boutin, C. Brandau, A. Brünle, P. Dendooven, G. Fehrenbacher, E. Floch, M. Gleim, W. Hüller, H. Iwase, A. Kalimov, C. Karagiannis, M. Kauschke, A. Kelic, B. Kindler, G. Klappich, E. Kozlova, A. Krämer, A. Kratz, T. Kubo, N. Kurz, K. Kusaka, H. Leibrock, J. Lettry, S. Litvinov, Y. Litvinov, B. Lommel, S. Manikonda, A. Marbs, G. Moritz, C. Mühle, C. Nociforo, J.A. Nolen, H. Penttilä, W. Plass, Z. Podolyak, A. Prochazka, I. Pschorn, T. Radon, H. Ramakers, H. Reich-Sprenger, J. Saren, G. Savard, C. Scheidenberger, P. Schnizer, M. Schwickert, B. Sherrill, B. Sitar, A. Stafinak, R. Stieglitz, M. Svedentsov, N. Tahir, A. Tauschwitz, O. Tarasov, M. Tomut, P. Vobly, H. Welker, R. Wilfinger, C. Will, J. Winfield, Y. Xiang, M. Yavor, A. Yoshida, A. Zeller, Technical design report on the super-FRS, Darmstadt, 2009.
[2] S. Péraire, P.R. Sala, Beam dumps and beam stoppers for LHC and CNGS transfer lines, Geneva, 2001. https://cds.cern.ch/record/487075/files/lhc-project-report-465.pdf (accessed August 15, 2018).
[3] M. Maslov, M. Schmitz, V. Sychev, Layout Considerations on the 25GeV / 300kW Beam Dump of the XFEL Project, 2006. http://flash.desy.de/reports_publications/tesla_fel_reports/tesla_fel_2006/e1129/infoboxContent1791/fel2006-05.pdf (accessed August 15, 2018).
[4] P. Sigmund, Particle Penetration and Radiation Effects, Springer Berlin Heidelberg, 2006, doi:10.1007/3-540-31718-X.
[5] D. Kiselev, R. Bergmann, D. Schumann, V. Talanov, M. Wohlmuther, Proton induced activity in graphite - Comparison between measurement and simulation, J. Phys. Conf. Ser. (2018) 1046, doi:10.1088/1742-6596/1046/1/012003.
[6] C. Hubert, K.O. Voss, M. Bender, K. Kupka, A. Romanenko, D. Severin, C. Trautmann, M. Tomut, Swift heavy ion-induced radiation damage in isotropic graphite studied by micro-indentation and in-situ electrical resistivity, Nucl. Instrum. Methods Phys. Res. Sect. B Beam Interact. Mater. Atoms 365 (2015) 509–514, doi:10.1016/j.nimb.2015.08.056.
[7] P. Zhai, J. Liu, J. Zeng, J. Duan, L. Xu, H. Yao, H. Guo, S. Zhang, M. Hou, Y. Sun, Evidence for re-crystallization process in the irradiated graphite with heavy ions obtained by Raman spectroscopy, Carbon N.Y. 101 (2016) 22–27, doi:10.1016/j.carbon.2016.01.076.
[8] S. Fernandes, F. Pellemoine, M. Tomut, M. Avilov, M. Bender, M. Boulesteix, M. Krause, W. Mittig, M. Schein, D. Severin, C. Trautmann, In-situ electric resistance measurements and annealing effects of graphite exposed to swift heavy ions, Nucl. Instrum. Methods Phys. Res. Sect. B Beam Interact. with Mater. Atoms 314 (2013) 125–129, doi:10.1016/j.nimb.2013.04.060.

[9] C. Hubert, Characterization of Radiation Damage Induced by Swift Heavy Ions in Graphite, TU Darmstadt, 2016 http://tuprints.ulb.tu-darmstadt.de/id/eprint/5466.

[10] F. Pellemoine, M. Avilov, M. Bender, R.C. Ewing, S. Fernandes, M. Lang, W.X. Li, W. Mittig, M. Schein, D. Severin, M. Tomut, C. Trautmann, F.X. Zhang, Study on structural recovery of graphite irradiated with swift heavy ions at high temperature, Nucl. Instrum. Methods Phys. Res. Sect. B Beam Interact. with Mater. Atoms 365 (2015) 522–524, doi:10.1016/j.nimb.2015.09.007.

[11] J.H.W. Simmons, Radiation Damage in Graphite, Pergamon Press, 1965.

[12] I.B. Mason, R.H. Knibbs, Influence of crystallite size on the thermal conductivity of irradiated polycrystalline graphite, Nature 198 (1963) 850–851 http://dx.doi.org/10.1038/198850a0.

[13] T. Maruyama, M. Harayama, Neutron irradiation effect on the thermal conductivity and dimensional change of graphite materials, J. Nucl. Mater. 195 (1992) 44–50, doi:10.1016/0022-3115(92)90362-O.

[14] S. Ishiyama, T.D. Burchell, J.P. Strizak, M. Eto, The effect of high fluence neutron irradiation on the properties of a fine-grained isotropic nuclear graphite, J. Nucl. Mater. 230 (1996) 1–7, doi:10.1016/0022-3115(96)00005-0.

[15] M.R. Ammar, N. Galy, J.N. Rouzaud, N. Toulhoat, C.E. Vaudey, P. Simon, N. Moncoffre, Characterizing various types of defects in nuclear graphite using Raman scattering: heat treatment, ion irradiation and polishing, Carbon N. Y. 95 (2015) 364–373, doi:10.1016/j.carbon.2015.07.095.

[16] A.A. Campbell, Y. Katoh, M.A. Snead, K. Takizawa, Property changes of G347A graphite due to neutron irradiation, Carbon N. Y. 109 (2016) 860–873, doi:10.1016/j.carbon.2016.08.042.

[17] R. Krishna, a.N. Jones, L. McDermott, B.J. Marsden, Neutron irradiation damage of nuclear graphite studied by high-resolution transmission electron microscopy and Raman spectroscopy, J. Nucl. Mater. 467 (2015) 557–565, doi:10.1016/j.jnucmat.2015.10.027.

[18] G.S. Was, Fundamentals of Radiation Materials Science, Springer, 2007.

[19] D.K. Avasthi, G.K. Mehta, Swift Heavy Ions for Materials Engineering and Nanostructuring, Springer, 2011.

[20] C. Trautmann, Micro- and Nanoengineering with Ion Tracks, in: R. Hellborg, H.J. Whitlow, Y. Zhang (Eds.), Ion Beams in Nanoscience and Technology, Springer Berlin Heidelberg, Berlin, Heidelberg, 2009, pp. 369–387, doi:10.1007/978-3-642-00623-4.

[21] W.J. Weber, Models and mechanisms of irradiation-induced amorphization in ceramics, Nucl. Instrum. Methods Phys. Res. Sect. B Beam Interact. Mater. Atoms 166 (2000) 98–106, doi:10.1016/S0168-583X(99)00643-6.

[22] L.L. Snead, T.D. Burchell, Thermal conductivity degradation of graphites due to nuetron irradiation at low temperature, J. Nucl. Mater. 224 (1995) 222–229, doi:10.1016/0022-3115(95)00071-2.

[23] E.I. Zhmurikov, I.V. Savchenko, S.V. Stankus, O.S. Yatsuk, L.B. Tecchio, Measurements of the thermophysical properties of graphite composites for a neutron target converter, Nucl. Instrum. Methods Phys. Res. Sect. A Accel. Spectrom Detect. Assoc. Equip. 674 (2012) 79–84, doi:10.1016/j.nima.2012.01.015.

[24] J. Habainy, Y. Lee, K.B. Surreddi, A. Prosvetov, P. Simon, S. Iyengar, Y. Dai, M. Tomut, Study of heavy ion beam induced damage in tungsten for high power target applications, Nucl. Instrum. Methods Phys. Res. Sect. B Beam Interact. Mater. Atoms 439 (2019) 7–16, doi:10.1016/j.nimb.2018.11.017.

[25] P.J. Newby, B. Canut, J.M. Bluet, S. Gomès, M. Isaiev, R. Burbelo, K. Termentzidis, P. Chantrenne, L.G. Fréchette, V. Lysenko, Amorphization and reduction of thermal conductivity in porous silicon by irradiation with swift heavy ions, J. Appl. Phys. 114 (2013) 4903, doi:10.1063/1.4812280.

[26] P.M. Almond, D.P. Patel, Photothermal Science and Techniques, Springer Netherlands, 1996.

[27] G. Hamaoui, N. Horny, Z. Hua, T. Zhu, J.-F. Robillard, A. Fleming, H. Ban, M. Chirtoc, Electronic contribution in heat transfer at metal-semiconductor and metal silicide-semiconductor interfaces, Sci. Rep. 8 (2018) 11352, doi:10.1038/s41598-018-29505-4.

[28] N. Horny, M. Chirtoc, A. Fleming, G. Hamaoui, H. Ban, Kapitza thermal resistance studied by high-frequency photothermal radiometry, Appl. Phys. Lett. (2016) 109, doi:10.1063/1.4959084.

[29] D. Trefon-Radziejewska, G. Hamaoui, M. Chirtoc, N. Horny, V. Smokal, A. Biitseva, O. Krupka, B. Derkowska-Zielinska, Thermophysical properties of methacrylic polymer films with guest-host and side-chain azobenzene, Mater. Chem. Phys. 223 (2019) 700–707, doi:10.1016/j.matchemphys.2018.11.054.

[30] G. Hamaoui, R. Dagher, Y. Cordier, A. Michon, S. Potiron, M. Chirtoc, N. Horny, Kapitza thermal resistance characterization of epitaxial graphene–SiC(0001) interface, Appl. Phys. Lett. 114 (2019) 221601, doi:10.1063/1.5092207.

[31] G. Hamaoui, N. Horny, C.L. Gomez-Heredia, J.A. Ramirez-Rincon, J. Ordonez-Miranda, C. Champeaux, F. Dumas-Bouchiat, J.J. Alvarado-Gil, Y. Ezzahri, K. Joulain, M. Chirtoc, Thermophysical characterisation of VO$_2$ thin films hysteresis and its application in thermal rectification, Sci. Rep. 9 (2019) 1–10, doi:10.1038/s41598-019-45436-0.

[32] B.K. Bein, S. Krueger, J. Pelzl, Photoacoustic analysis of graphite limiters - changes in the thermal properties due to plasma limiter interaction, J. Nucl. Mater. 145–147 (1987) 458–462, doi:10.1016/0022-3115(87)90381-3.

[33] J. Pelzl, B.K. Bein, Photothermal characterization of plasma surface modifications, Pure Appl. Chem. 64 (1992) 739–744, doi:10.1351/pac199264050739.

[34] C. Jensen, M. Chirtoc, N. Horny, J.S. Antoniow, H. Pron, H. Ban, Thermal conductivity profile determination in proton-irradiated ZrC by spatial and frequency scanning thermal wave methods, J. Appl. Phys. (2013) 114, doi:10.1063/1.4821432.

[35] I. Suarez-Martinez, N.a. Marks, Effect of microstructure on the thermal conductivity of disordered carbon, Appl. Phys. Lett. 99 (2011) 1–4, doi:10.1063/1.3607872.

[36] L.D.S. Oliveira, P.A. Greaney, Thermal resistance from irradiation defects in graphite, Comput. Mater. Sci. 103 (2015) 68–76, doi:10.1016/j.commatsci.2015.03.001.

[37] R.A. Rymzhanov, S.A. Gorbunov, N. Medvedev, A.E. Volkov, Damage along swift heavy ion trajectory, Nucl. Instrum. Methods Phys. Res. Sect. B Beam Interact. Mater. Atoms 440 (2019) 25–35, doi:10.1016/j.nimb.2018.11.034.

[38] K. Kupka, A.A. Leino, W. Ren, H. Vázquez, E.H. Åhlgren, K. Nordlund, M. Tomut, C. Trautmann, P. Kluth, M. Toulemonde, F. Djurabekova, Graphitization of amorphous carbon by swift heavy ion impacts: molecular dynamics simulation, Diam. Relat. Mater. 83 (2018) 134–140, doi:10.1016/j.diamond.2018.01.015.

[39] H.J. Christie, D.L. Roach, I. Suarez-Martinez, N.A. Marks, M. Robinson, D.K. Ross, Simulating radiation damage cascades in graphite, Carbon N. Y. 81 (2014) 105–114, doi:10.1016/j.carbon.2014.09.031.

[40] SGL Group, SIGRAFINE R6650 datasheet, (n.d.). https://www.sglgroup.com/cms/_common/downloads/products/product-groups/gs/tds/iso/SIGRAFINE_TDS-R6650.02.pdf (accessed July 17, 2018).

[41] HTW Hochtemperatur-Werkstoffe GmbH, HTW Germany. SIGRADUR datasheet, (n.d.). http://htw-germany.com/technology.php5?lang=en&nav0=2&nav1=16 (accessed August 9, 2018).

[42] J.F. Ziegler, M.D. Ziegler, J.P. Biersack, SRIM – The stopping and range of ions in matter (2010), Nucl. Instrum. Methods Phys. Res. Sect. B Beam Interact. Mater. Atoms. 268 (2010) 1818–1823, doi:10.1016/j.nimb.2010.02.091.

[43] P. Grossel, F. Depasse, Alternating heat diffusion in thermophysical depth profiles: multilayer and continuous descriptions, J. Phys. D. Appl. Phys. 31 (1998) 216–223, doi:10.1088/0022-3727/31/2/007.

[44] M. Chirtoc, Investigation of layered systems by photothermal methods with periodic excitation, in: E.M. Moares (Ed.), Thermal Wave Physics and Related Photothermal Techniques: Basic Principles and Recent Developments, Transworld Research Network, 2009, p. 29.

[45] W.J. Parker, R.J. Jenkins, C.P. Butler, G.L. Abbott, Flash method of determining thermal diffusivity, heat capacity, and thermal conductivity, J. Appl. Phys. 32 (1961) 1679–1684, doi:10.1063/1.1728417.

[46] L. Vozár, W. Hohenauer, Flash method of measuring the thermal diffusivity. A review, High Temp. - High Press 35–36 (2003) 253–264, doi:10.1068/htjr119.

[47] R.D. Cowan, Pulse method of measuring thermal diffusivity at high temperatures, J. Appl. Phys. 34 (1963) 926–927, doi:10.1063/1.1729564.

[48] P. Hui, H.S. Tan, Modelling of thermal diffusivity measurement of diamond thin films using a pulsed laser technique, Surf. Coatings Technol. 62 (1993) 361–366, doi:10.1016/0257-8972(93)90268-S.

[49] A. Ferrari, J. Robertson, Interpretation of Raman spectra of disordered and amorphous carbon, Phys. Rev. B. 61 (2000) 14095–14107, doi:10.1103/PhysRevB.61.14095.

[50] L.G. Cançado, A. Jorio, E.H. Martins Ferreira, F. Stavale, C. Achete, R.B. Capaz, M.V.O. Moutinho, A. Lombardo, T.S. Kulmala, A.C. Ferrari, L.G. Cançado, a. Jorio, E.H.M. Ferreira, F. Stavale, C.a. Achete, R.B. Capaz, M.V.O. Moutinho, a. Lombardo, T.S. Kulmala, a.C. Ferrari, Quantifying defects in graphene via Raman spectroscopy at different excitation energies, Nano Lett. 11 (2011) 3190–3196, doi:10.1021/NL201432G.

[51] K. Niwase, Raman spectroscopy for quantitative analysis of point defects and defect clusters in irradiated graphite, Int. J. Spectrosc. 2012 (2012) 1–14, doi:10.1155/2012/197609.

[52] A. Sadezky, H. Muckenhuber, H. Grothe, R. Niessner, U. Pöschl, Raman microspectroscopy of soot and related carbonaceous materials: spectral analysis and structural information, Carbon N. Y. 43 (2005) 1731–1742, doi:10.1016/j.carbon.2005.02.018.

[53] M. Pawlyta, J.N. Rouzaud, S. Duber, Raman microspectroscopy characterization of carbon blacks: spectral analysis and structural information, Carbon N. Y. 84 (2015) 479–490, doi:10.1016/j.carbon.2014.12.030.

[54] P.J.F. Harris, Fullerene-related structure of commercial glassy carbons, Philos. Mag. 84 (2004) 3159–3167, doi:10.1080/14786430410001720363.

[55] K. Jurkiewicz, S. Duber, H.E. Fischer, A. Burian, Modelling of glass-like carbon structure and its experimental verification by neutron and X-ray diffraction, J. Appl. Crystallogr. 50 (2017) 36–48, doi:10.1107/S1600576716017660.

[56] K. Jurkiewicz, M. Pawlyta, D. Zygadło, D. Chrobak, S. Duber, R. Wrzalik, A. Ratuszna, A. Burian, Evolution of glassy carbon under heat treatment: correlation structure–mechanical properties, J. Mater. Sci. 53 (2018) 3509–3523, doi:10.1007/s10853-017-1753-7.

[57] S. Sharma, C.N. Shyam Kumar, J.G. Korvink, C. Kübel, Evolution of glassy carbon microstructure: in situ transmission electron microscopy of the pyrolysis process, Sci. Rep. 8 (2018) 1–12, doi:10.1038/s41598-018-34644-9.

[58] M.M. Lucchese, F. Stavale, E.H.M. Ferreira, C. Vilani, M.V.O. Moutinho, R.B. Capaz, C.a. Achete, a. Jorio, Quantifying ion-induced defects and Raman relaxation length in graphene, Carbon N. Y. 48 (2010) 1592–1597, doi:10.1016/j.carbon.2009.12.057.

[59] J. Zeng, J. Liu, H.J. Yao, P.F. Zhai, S.X. Zhang, H. Guo, P.P. Hu, J.L. Duan, D. Mo, M.D. Hou, Y.M. Sun, Comparative study of irradiation effects in graphite and graphene induced by swift heavy ions and highly charged ions, Carbon N. Y. 100 (2016) 16–26, doi:10.1016/j.carbon.2015.12.101.

[60] J. Zeng, H.J. Yao, S.X. Zhang, P.F. Zhai, J.L. Duan, Y.M. Sun, G.P. Li, J. Liu, Swift heavy ions induced irradiation effects in monolayer graphene and highly oriented pyrolytic graphite, Nucl. Instrum. Methods Phys. Res. Sect. B Beam Interact. Mater. Atoms 330 (2014) 18–23, doi:10.1016/j.nimb.2014.03.019.

[61] D.G. McCulloch, S. Prawer, A. Hoffman, Structural investigation of xenon-ion-beam-irradiated glassy carbon, Phys. Rev. B. 50 (1994) 5905–5917, doi:10.1103/PhysRevB.50.5905.

[62] W.J. Weber, E. Zarkadoula, O.H. Pakarinen, R. Sachan, M.F. Chisholm, P. Liu, H. Xue, K. Jin, Y. Zhang, Synergy of elastic and inelastic energy loss on ion track formation in SrTiO$_3$, Sci. Rep. 5 (2015), doi:10.1038/srep07726.

[63] E. Zarkadoula, H. Xue, Y. Zhang, W.J. Weber, Synergy of inelastic and elastic energy loss: temperature effects and electronic stopping power dependence, Scr. Mater. 110 (2016) 2–5, doi:10.1016/j.scriptamat.2015.05.044.

[64] N. Sellami, M.L. Crespillo, Y. Zhang, W.J. Weber, Two-stage synergy of electronic energy loss with defects in LiTaO$_3$ under ion irradiation, Mater. Res. Lett. 6 (2018) 339–344, doi:10.1080/21663831.2018.1455753.

[65] K. Jin, Y. Zhang, W.J. Weber, Synergistic effects of nuclear and electronic energy deposition on damage production in KTaO$_3$, Mater. Res. Lett. 6 (2018) 531–536, doi:10.1080/21663831.2018.1495131.

[66] L. Thomé, A. Debelle, F. Garrido, S. Mylonas, B. Décamps, C. Bachelet, G. Sattonnay, S. Moll, S. Pellegrino, S. Miro, P. Trocellier, Y. Serruys, G. Velisa, C. Grygiel, I. Monnet, M. Toulemonde, P. Simon, J. Jagielski, I. Jozwik-Biala, L. Nowicki, M. Behar, W.J. Weber, Y. Zhang, M. Backman, K. Nordlund, F. Djurabekova, Radiation effects in nuclear materials: role of nuclear and electronic energy losses and their synergy, Nucl. Instrum. Methods Phys. Res. Sect. B Beam Interact. Mater. Atoms 307 (2013) 43–48, doi:10.1016/j.nimb.2012.11.077.

[67] M. Chirtoc, Thermal wave physics and related photothermal techniques: basic principles and recent developments, in: E. Marin (Ed.), Therm. Wave Phys. Relat. Photothermal Tech. Basic Princ. Recent Dev., Transworld Research Network, 2009, p. 29.

[68] D. Maillet, S. André, J.C. Batsale, A. Degiovanni, C. Moyne, Thermal Quadrupoles : Solving the Heat Equation Through Integral Transforms, John Wiley and Sons Ltd, 2000.

[69] J. Yang, E. Ziade, A.J. Schmidt, Uncertainty analysis of thermoreflectance measurements, Rev. Sci. Instrum. 87 (2016) 14901, doi:10.1063/1.4939671.

[70] B. März, K. Jolley, R. Smith, H. Wu, Near-surface structure and residual stress in as-machined synthetic graphite, Mater. Des. 159 (2018) 103–116, doi:10.1016/j.matdes.2018.08.041.

[71] I. Manika, J. Maniks, R. Zabels, J. Gabrusenoks, M. Krause, M. Tomut, K. Schwartz, Nanoindentation and raman spectroscopic study of graphite irradiated with swift 238U ions, Fuller. Nanotub Carbon Nanostruct. 20 (2012) 548–552, doi:10.1080/1536383X.2012.656064.

[72] M. Tomut, B. Achenbach, K.H. Behr, W. Ensinger, H. Geissel, A. Hübner, A. Keli, B. Kindler, M. Krause, B. Lommel, I. Manika, R. Neumann, C. Scheidenberger, K. Schwartz, K. Sümmerer, C. Trautmann, H. WeicK, M. Winkler, Experimental investigations on heavy-ion induced radiation damage of graphite for the super-frs target and beam catchers, in: K. Große (Ed.), GSI Scientific Reports 2007, GSI, Darmstadt, 2008, p. 69. http://repository.gsi.de/record/53524.

[73] M. Toulemonde, W. Assmann, C. Dufour, a. Meftah, C. Trautmann, Nanometric transformation of the matter by short and intense electronic excitation: experimental data versus inelastic thermal spike model, Nucl. Instrum. Methods Phys. Res. Sect. B Beam Interact. Mater. Atoms 277 (2012) 28–39, doi:10.1016/j.nimb.2011.12.045.

[74] J. Liu, R. Neumann, C. Trautmann, C. Müller, Tracks of swift heavy ions in graphite studied by scanning tunneling microscopy, Phys. Rev. B. 64 (2001) 184115 doi:Artn 184115\nDoi, doi:10.1103/Physrevb.64.184115.

[75] C.H. Wu, J.P. Bonal, B. Kryger, The effect of high-dose neutron irradiation on the properties of graphite and silicon carbide, J. Nucl. Mater. 208 (1994) 1–7, doi:10.1016/0022-3115(94)90191-0.

[76] G. Fugallo, A. Cepellotti, L. Paulatto, M. Lazzeri, N. Marzari, F. Mauri, Thermal conductivity of graphene and graphite: collective excitations and mean free paths, Nano Lett. 14 (2014) 6109–6114, doi:10.1021/nl502059f.

[77] A.A. Balandin, Thermal properties of graphene and nanostructured carbon materials, Nat. Mater. 10 (2011) 569, doi:10.1038/nmat3064.

[78] D.F. Pedraza, P.G. Klemens, Effective conductivity of polycrystalline graphite, Carbon N. Y. 31 (1993) 951–956, doi:10.1016/0008-6223(93)90197-I.

[79] P.G. Klemens, D.F. Pedraza, Thermal conductivity of graphite in the basal plane, Carbon N. Y. 32 (1994) 735–741, doi:10.1016/0008-6223(94)90096-5.

[80] H. Zhang, X. Chen, Y.-D. Jho, A.J. Minnich, Temperature dependent mean free path spectra of thermal phonons along the c-axis of graphite, Nano Lett 16 (2016) 1643–1649. 10.1021/acs.nanolett.5b04499

[81] Z.G. Fthenakis, Z. Zhu, D. Tománek, Effect of structural defects on the thermal conductivity of graphene: from point to line defects to haeckelites, Phys. Rev. B - Condens. Matter Mater. Phys. 89 (2014) 1–6, doi:10.1103/PhysRevB.89.125421.

[82] R.E. Stoller, M.B. Toloczko, G.S. Was, A.G. Certain, S. Dwaraknath, F.A. Garner, On the use of SRIM for computing radiation damage exposure, Nucl. Instrum. Methods Phys. Res. Sect. B Beam Interact. Mater. Atoms 310 (2013) 75–80, doi:10.1016/j.nimb.2013.05.008.

[83] A.J. McKenna, T. Trevethan, C.D. Latham, P.J. Young, M.I. Heggie, Threshold displacement energy and damage function in graphite from molecular dynamics, Carbon N. Y. 99 (2016) 71–78, doi:10.1016/j.carbon.2015.11.040.